

Distribution of Damped Lyman- α Absorbers in a Λ Cold Dark Matter Universe

Kentaro Nagamine¹, Arthur M. Wolfe¹, Lars Hernquist², Volker Springel³

ABSTRACT

We examine the ‘rate-of-incidence’ distribution for damped Lyman- α absorbers (DLAs) as a function of halo mass, galaxy apparent magnitude, and impact parameter using a series of cosmological Smoothed Particle Hydrodynamics (SPH) simulations. Our simulations include radiative cooling and heating by a UV background, star formation, and feedback from supernovae and galactic winds. We find the DLA rate-of-incidence in our simulations at $z = 3$ is dominated (80 – 90%) by faint galaxies with apparent magnitude $\mathcal{R}_{AB} < 25.5$. However, interestingly in a ‘strong wind’ run, we find that the differential distribution of DLA sight-lines is peaked at $M_{\text{halo}} = 10^{12} h^{-1} M_{\odot}$ ($\mathcal{R}_{AB} \simeq 27$) and the mean DLA halo mass is $\langle M_{\text{DLA}} \rangle = 10^{12.4} h^{-1} M_{\odot}$ ($\mathcal{R}_{AB} \simeq 26$). These mass-scales are much larger than those if we ignore winds, because galactic feedback suppresses the DLA cross section in low mass halos and increases the relative contribution to the DLA incidence from more massive halos. But we caution that the mean DLA mass is biased towards a high value and is very different from the median halo mass unless the DLA distribution is highly peaked. The simulations also suggest that DLAs at $z = 3$ are more compact than present-day disk galaxies, and the impact parameter distribution is very narrow unless we limit searches for the galaxy hosting a DLA to only bright Lyman-break galaxies (LBGs). We find that the comoving number density of DLAs is higher than that of LBGs down to the magnitude limit of $\mathcal{R}_{AB} = 30$ mag if the physical radius of each DLA is smaller than $5 h_{70}^{-1}$ kpc. We discuss conflicts between current simulations and observations, and potential problems with hydrodynamic simulations based on the cold dark matter model.

Subject headings: quasars: absorption lines — galaxies: ISM — stars: formation — galaxies: evolution — galaxies: formation — methods: numerical

¹University of California, San Diego, Center for Astrophysics and Space Sciences, CA 92093-0424, U.S.A.

²Harvard University, 60 Garden Street, Cambridge, MA 02138, U.S.A.

³Max-Planck-Institut für Astrophysik, Karl-Schwarzschild-Straße 1, 85740 Garching bei München, Germany

1. Introduction

Within the currently favored hierarchical Λ cold dark matter (CDM) model, damped Lyman- α absorbers¹ observed in high redshift quasar absorption lines are considered to arise from radiatively cooled neutral gas in dark matter halos. They are known to dominate the neutral hydrogen mass density at high redshift (e.g., Lanzetta et al. 1995; Storrie-Lombardi & Wolfe 2000), and hence provide a significant reservoir of cold neutral gas for star formation. If this picture is correct, then DLAs are closely linked to star formation and must be located inside or in the vicinity of galaxies within dark matter halos (hereafter often just ‘halos’). For these reasons, DLAs provide an excellent probe of high redshift galaxy formation that complements the study of high redshift galaxies by the direct observation of stellar light.

Despite significant observational effort over the years (e.g., Wolfe et al. 1986; Lanzetta et al. 1995; Wolfe et al. 1995; Storrie-Lombardi & Wolfe 2000; Rao & Turnshek 2000; Prochaska et al. 2001; Prochaska & Wolfe 2002; Péroux et al. 2003; Chen & Lanzetta 2003), the true nature of DLA galaxies (i.e., galaxies that host DLAs) is still uncertain, and it is unclear how DLAs are distributed among dark matter halos. The observed large velocity widths of low-ionization lines support a large, thick disk hypothesis (e.g., Wolfe et al. 1986; Turnshek et al. 1989; Prochaska & Wolfe 1997, 1998), while at the same time there is evidence that a wider range of galaxies could be DLA galaxies (e.g., Le Brun et al. 1997; Kulkarni et al. 2000, 2001; Rao & Turnshek 2000; Chen & Lanzetta 2003; Weatherley et al. 2005). Haehnelt, Steinmetz, & Rauch (1998) also showed that their SPH simulations were able to reproduce the observed asymmetric profiles of low-ionization absorption lines, and therefore argued that DLAs could be protogalactic gas clumps rather than well-developed massive disks that have settled down. But their simulations did not include the effects of energy and momentum feedback owing to star formation, and they only analyzed a few systems.

To interpret observations of DLAs, it is useful to define the ‘rate-of-incidence’ distribution as a function of halo mass or associated galaxy magnitude. The ‘rate-of-incidence’ of DLAs (often just ‘DLA incidence’), dN/dz , i.e., the probability of finding a DLA along a line-of-sight per unit redshift, could either be dominated by low-mass halos, or by very massive halos. In the former case, the DLA cross section in low-mass halos is significant, and because the halo mass function in a CDM universe is a steeply increasing function with decreasing halo mass, the net contribution to the DLA rate-of-incidence from low-mass halos dominates that from massive halos. One of the critical elements that needs to be determined is the DLA cross section as a function of halo mass.

¹DLas are historically defined to be absorption systems with neutral hydrogen column densities $N_{\text{HI}} > 2 \times 10^{20} \text{ cm}^{-2}$ (Wolfe et al. 1986).

Many authors have used semi-analytic models of galaxy formation based on the hierarchical CDM model to study the distribution of DLAs. Mo et al. (1998) improved the model of Kauffmann (1996) to study the formation of disk galaxies by following the angular momentum distribution, and examined the distribution of DLA rate-of-incidence as a function of halo circular velocity and impact parameter. While these calculations provide insights on what is expected in hierarchical CDM models, they rely on assumptions about the mass fraction of disks and the geometry of the gas distribution relative to those of dark matter halos. Also they are not able to directly account for dynamical effects from violent merging of halos/galaxies and associated heating/cooling of gas. Haehnelt et al. (2000) studied the luminosity and impact parameter distribution of DLAs using simple scaling relationships from both observations and simulations and an analytic halo mass function. More recently, Maller et al. (2001) discussed the distribution of DLAs based on the semi-analytic model of Somerville et al. (2001). Okoshi et al. (2004) and Okoshi & Nagashima (2005) also examined the chemical evolution and properties of DLAs at $z \leq 1$ based on the semianalytic model of Nagashima et al. (2001). While these comprehensive semianalytic models did not require assumptions about the cold gas mass fraction in halos, they still had to adopt choices for the geometry of the gas distribution, such as an exponential radial profile of H I column density in the case of Okoshi et al. (2004), focusing on the virialized systems. We will compare our results in this paper to those of the above authors in what follows.

On the other hand, numerical simulations are able to describe dynamical effects in a more realistic manner than semi-analytic models, but instead have resolution and box-size limitations owing to finite computational resources. State-of-the-art cosmological hydrodynamic simulations that evolve comoving volumes larger than $\sim (10 h^{-1} \text{ Mpc})^3$ can now achieve a spatial resolution of $\sim 1 \text{ kpc}$ in comoving coordinates, but have the fundamental problem of being unable to produce a large population of realistic disk galaxies with the observed number density at $z = 0$ (e.g., Robertson et al. 2004). Even so, implementations of the physics of star formation and feedback have greatly improved over the past several years (e.g., Springel & Hernquist 2002, 2003a,b; Cen et al. 2004), therefore it is of interest to compare results with those obtained from simulations that did not include star formation and feedback (Haehnelt et al. 1998).

In an earlier paper, Nagamine, Springel, & Hernquist (2004a) studied the neutral hydrogen mass density, column density distribution, DLA cross section, and the rate-of-incidence using a series of SPH simulations with varying box size and feedback strength. One of their results was that the DLA cross section in low-mass halos depends on both resolution and the feedback strength in individual simulations. This results in a strong variation in the distribution of DLA incidence which was often neglected in other numerical studies (Katz et al. 1996b; Gardner et al. 1997a,b, 2001). Nagamine, Springel, & Hernquist (2004b) also

investigated the star formation rate and metallicity distribution of DLAs in the same series of cosmological SPH simulations. In this paper we extend our work by computing the rate-of-incidence distribution for DLAs as a function of dark matter halo mass, apparent magnitude of DLA galaxies, and impact parameter in the same simulations used by Nagamine et al. (2004a,b), and focus on the issue of “Which dark matter halos are most responsible for the DLAs?”. We will also discuss some tension found between the simulation results and new observations by Prochaska et al. (2005) that are derived from the Sloan Digital Sky Survey (SDSS) Data Release 3.

2. Simulations

We use the GADGET-2 code (Springel et al. 2001; Springel 2005) which employs the Smoothed Particle Hydrodynamics (SPH) technique. It adopts the entropy-conservative formulation of Springel & Hernquist (2002) which largely alleviates the overcooling problem that the previous generation of SPH codes suffered. Our simulations include radiative cooling and heating with a uniform UV background of a modified Haardt & Madau (1996) spectrum (Katz et al. 1996a; Davé et al. 1999), star formation, supernova feedback, a phenomenological model for galactic winds (Springel & Hernquist 2003b), and a sub-resolution multiphase model of the ISM (Springel & Hernquist 2003a).

We use a series of simulations of varying box-size and particle number (see Table 1) in order to assess the impact of numerical resolution on our results. Also, the strength of galactic wind feedback is varied among the O3 (no wind), P3 (weak wind), and Q3 (strong wind) runs, allowing us to study the consequences of feedback on our results. The adopted cosmological parameters of all runs are $(\Omega_m, \Omega_\Lambda, \Omega_b, \sigma_8, h) = (0.3, 0.7, 0.04, 0.9, 0.7)$. We also use the notation $h_{70} = h/0.7$ when we discuss the impact parameter distribution, where h is the Hubble parameter in units of $100 \text{ km s}^{-1} \text{ Mpc}^{-1}$. In this paper, we only use simulations with a box-size of $10h^{-1} \text{ Mpc}$ in order to achieve high spatial resolution, and focus on $z = 3$ since this is one of the epochs where the largest observational data sets are available and hence more accurate comparisons to observations are possible.

3. Rate-of-incidence as a function of halo mass

Nagamine et al. (2004a) estimated the relationship between the *total* DLA cross section $\sigma_{\text{DLA}}^{\text{co}}$ (in units of comoving $h^{-2} \text{ kpc}^2$; note that Fig. 2 – 4 of Nagamine et al. (2004a) plotted

comoving $h_{70}^{-2} \text{ kpc}^2$) and the dark matter halo mass (in units of $h^{-1}M_\odot$) at $z = 3$ as

$$\log \sigma_{\text{DLA}}^{\text{co}} = \alpha (\log M_{\text{halo}} - 12) + \beta, \quad (1)$$

with slopes $\alpha = 0.72, 0.79, 0.84, 0.93, 1.02$ and the normalization $\beta = 3.94, 3.99, 3.98, 4.03, 4.18$ for the O3, P3, Q3, Q4, and Q5 runs. The slope α is always positive, and the massive halos have larger DLA cross section, but they are more scarce compared to less massive halos. The quantity β gives the value of $\log \sigma_{\text{DLA}}^{\text{co}}$ at $M_{\text{halo}} = 10^{12} h^{-1}M_\odot$. This reference mass-scale was chosen because it was well covered by most of the simulations used in their paper. Two qualitative trends can be read off: (1) As the strength of galactic wind feedback increases (from O3 to Q3 run), the slope α becomes steeper while the normalization β remains roughly constant. This is because a stronger wind reduces the gas in low-mass halos at a higher rate by ejecting the gas out of the potential well of the halo. (2) As the numerical resolution is improved (from Q3 to Q5 run), both the slope and the normalization increase. This is because with higher resolution, star formation in low-mass halos can be described better and as a result the neutral gas content is decreased due to winds. On the other hand, a lower resolution run misses the early generation of halos and the neutral gas in them.

Nagamine et al. (2004a) studied the cumulative distribution of DLA rate-of-incidence, but here we study the differential distribution instead. The differential distribution function of DLA incidence can be computed as

$$\frac{dN_{\text{DLA}}}{dz d \log M} = \frac{dr}{dz} [M n(M, z) \ln(10)] \sigma_{\text{DLA}}^{\text{co}}(M, z), \quad (2)$$

where $n(M, z)$ is the dark matter halo mass function, and $dr/dz = c/H(z)$ with $H(z) = H_0 E(z) = H_0 \sqrt{\Omega_m(1+z)^3 + \Omega_\Lambda}$ for a flat universe. We use the Sheth & Tormen (1999) parametrization for $n(M)$ as shown in Figure 1. Note that the dependence on the Hubble constant disappears on the right-hand-side of Equation (2) because dr/dz scales as h^{-1} , $M n(M)$ scales as h^3 , and σ_{DLA} scales as h^{-2} in the simulation. For the cumulative version of this calculation, see Equation (8) and Figure 5 of Nagamine et al. (2004a). Equation (2) can be derived from the following expression for the DLA area covering fraction on the sky along the line element $c dt$:

$$dN_{\text{DLA}} = n_{\text{phys}}(M) dM \cdot \sigma_{\text{DLA}}^{\text{phys}} \cdot c dt \quad (3)$$

$$= (1+z)^3 n_{\text{co}}(M) dM \cdot \sigma_{\text{DLA}}^{\text{phys}} \cdot a dr \quad (4)$$

$$= n_{\text{co}}(M) dM \cdot \sigma_{\text{DLA}}^{\text{co}} \cdot dr, \quad (5)$$

where we have used $c dt = a dr$ and $\sigma_{\text{DLA}}^{\text{co}} = (1+z)^2 \sigma_{\text{DLA}}^{\text{phys}}$. Here a is the scale factor, dr is the line element in comoving coordinate, and $n_{\text{co}}(M) dM$ and $n_{\text{phys}}(M) dM$ are the comoving and physical number density of halos in the mass range $[M, M+dM]$, respectively.

Sometimes the ‘absorption distance’ $dX \equiv \frac{H_0}{c} (1+z)^3 c dt = \frac{H_0}{c} (1+z)^2 dr = \frac{H_0}{H(z)} (1+z)^2 dz = (1+z)^2 dz/E(z)$ is defined, and is used to express the rate-of-incidence as

$$\frac{dN_{\text{DLA}}}{dX} = \frac{c}{H_0} n_{\text{co}}(M) dM \cdot \sigma_{\text{DLA}}^{\text{phys}}. \quad (6)$$

For $z = 3$ and our adopted cosmology, $dX/dz = 3.5867$. In Equations (3) to (6), we left in the dependence on halo masses explicitly, but in practice an integral over a certain range of halo mass has to be performed when comparing with actual observations.

We now use the power-law fits for $\sigma_{\text{DLA}}^{\text{co}}(M, z)$ described above to compute the differential distribution of DLA incidence via Equation (2). The result is shown in Figure 2 for all the simulations at $z = 3$. The qualitative features of the curves are easy to understand. Because $n(M) \propto M^{-2}$ at $M \approx 10^8 - 10^{12} h^{-1} M_{\odot}$ (see Figure 1), the distribution is flat when $\sigma_{\text{DLA}} \propto M$. In fact, $n(M)$ is slightly shallower than M^{-2} (more like $M^{-1.8}$), therefore the distribution for the P3 run is almost flat at $10^8 < M < 10^{12} h^{-1} M_{\odot}$, because $\sigma_{\text{DLA}} \propto M^{0.79}$ in this simulation. At masses higher than $10^{12} h^{-1} M_{\odot}$, the mass function deviates from the M^{-2} power-law significantly, and the distributions for all runs quickly drop off to a small value.

The halo masses where each distribution peaks are listed in the second column of Table 2. The peak halo mass M_{peak} becomes larger as the feedback strength increases. For the O3 run, we indicated $M_{\text{peak}} = 10^{8.5} h^{-1} M_{\odot}$ in parentheses because we think that the DLA cross section rapidly fall off at this halo mass based on the work by Nagamine et al. (2004a) and the peak halo mass is simply this cutoff mass-scale. The peak halo mass is significantly larger for the Q4 ($M_{\text{peak}} = 10^{11.6} h^{-1} M_{\odot}$) and Q5 ($M_{\text{peak}} = 10^{12} h^{-1} M_{\odot}$) runs compared to other runs.

4. Mean & Median halo masses of DLAs

For each simulation, we compute the mean DLA halo mass of the distribution shown in Figure 2 as

$$\langle M_{\text{DLA}} \rangle = \frac{\int_0^{\infty} M \frac{dN}{dz d \log M} d \log M}{\int_0^{\infty} \frac{dN}{dz d \log M} d \log M} \quad (7)$$

$$= \frac{\int_0^{\infty} M^2 n(M) \sigma_{\text{DLA}}(M) d \log M}{\int_0^{\infty} M n(M) \sigma_{\text{DLA}}(M) d \log M}, \quad (8)$$

and the result of this calculation is summarized in Table 2. The mean halo mass is smaller for the ‘no-wind’ (O3) run, and is larger for the ‘strong-wind’ (Q3 to Q5) runs. This is because of

the steepening of the relationship between σ_{DLA} and M_{halo} as the feedback strength increases. But the mean halo mass is in the range $M_{\text{DLA}} = 10^{11.5} - 10^{12.5} h^{-1} M_{\odot}$ for all runs. While this mass-scale is not as large as a Milky Way sized halo ($M_{\text{halo}} \simeq 10^{12} - 10^{13} M_{\odot}$), it is certainly more massive than that of dwarf galaxies. We also list the mean of $\log M_{\text{DLA}}$ for comparison with the results by Bouche et al. (2005). We will discuss the implications of these mass-scales in Section 8.

One can also look at the median halo mass M_{50} , below (or above) which 50 percent of the DLA rate-of-incidence is covered. The quantity M_{50} is defined by the following equation:

$$0.5 = \int_{M_{50}}^{\infty} n(M) \sigma_{\text{DLA}}(M) dM / \int_0^{\infty} n(M) \sigma_{\text{DLA}}(M) dM. \quad (9)$$

The median halo mass is always smaller than $\langle M_{\text{DLA}} \rangle$ for all runs. The values of M_{50} are indicated by the open cross in Figure 2, and $\langle M_{\text{DLA}} \rangle$ are indicated by the filled squares. We emphasize that M_{50} is much smaller than $\langle M_{\text{DLA}} \rangle$, and that $\langle M_{\text{DLA}} \rangle$ could be biased towards a large value because of the weighting by the halo mass; i.e., $M_{50} \neq \langle M_{\text{DLA}} \rangle$.

Furthermore, in Table 2 we also give the 75 percentile halo mass M_{75} , below which 75 percent of the DLA incidence is covered. For example, in the Q5 run, halos with masses $M_{\text{halo}} < 10^{12.3} h^{-1} M_{\odot}$ are responsible for 75% of the DLA incidence at $z = 3$. The values of M_{75} are shown with open triangles in Figure 2.

5. Luminosity distribution of DLA galaxies

The luminosity distribution of DLA galaxies constrains their nature, facilitating the interpretation of observations of DLA galaxies. Nagamine et al. (2004d) computed the spectra of all galaxies in the same simulations used in this paper from the population synthesis model of Bruzual & Charlot (2003, hereafter BClib03) based on the stellar mass, formation time, and metallicity of each stellar particle that makes up simulated galaxies. Using the computed spectra, we sum up the monochromatic luminosity at rest frame 1655Å (chosen because it corresponds to the observed-frame \mathcal{R} band of the $U_nG\mathcal{R}$ system) of all galaxies that are contained within the maximum radius of each dark matter halo identified by the friends-of-friends grouping algorithm (Davis et al. 1985), and compute the absolute AB magnitude at 1655Å using the following formula (see Equation (2) of Nnight et al. 2005) because BClib outputs its spectrum L_{λ} in units of $L_{\odot} \text{Å}^{-1}$, where $L_{\odot} = 3.826 \times 10^{33} \text{ erg s}^{-1}$ is the bolometric solar luminosity:

$$M_{AB} = -2.5 \log(\lambda^2 L_{\lambda}) + 13.83. \quad (10)$$

Figure 3 shows the relationship between M_{AB} and the halo mass for O3, P3, Q3, and Q5 runs at $z = 3$. The three dashed lines correspond to

$$M_{AB} = -2.5 (\log M_{\text{halo}} - 12) - C_1, \quad (11)$$

where $C_1 = 23.5, 22.5$, and 21.5 from top to bottom, and M_{halo} is in units of $h^{-1} M_{\odot}$. From Figure 3, we adopt $C_1 = 23.5$ for the O3 run, $C_1 = 22.5$ for the P3 run, and $C_1 = 21.5$ for the Q3 and Q5 runs. This figure shows that, on average, the galaxies in the ‘no-wind’ run (O3) are brighter than those in the ‘strong-wind’ run (Q3 & Q5) by about a factor of six. This was pointed out in Figure 6 of Nagamine et al. (2004d) and was attributed to the suppression of star formation by a strong galactic wind.

Here, the apparent and absolute magnitudes are related to each other as

$$m_{AB} = M_{AB} + 2.5 \log(1 + z) + 5 \log(d_L/10\text{pc}), \quad (12)$$

where d_L is the luminosity distance. Notice the positive sign in front of the 2nd term (which is normally negative); this is because of the definition of M_{AB} in Equation (10) (see also Equation (2) of Night et al. 2005). Inserting Equation (11) into Equation (12) and using $d_L(z = 3) = 2.542 \times 10^4 h_{70}^{-1} \text{Mpc}$ for our flat Λ cosmology, we obtain the relation between the apparent magnitude \mathcal{R}_{AB} and the halo mass M_{halo} as

$$\mathcal{R}_{AB} = -2.5 \log M_{\text{halo}} + C_2 - 5 \log h_{70}, \quad (13)$$

where $C_2 = 55.03$ (O3 run), 56.03 (P3 run), and 57.03 (Q3 and Q5 run), and M_{halo} is in units of $h^{-1} M_{\odot}$. These numerical values are consistent with the ones adopted by Haehnelt et al. (2000), where they assumed $m_{AB} = 26.6 - 7.5 \log(v_c/200 \text{ km s}^{-1}) = -2.5 \log M_{\text{halo}} + 55.7$ for a flat Λ cosmology. The circular velocity v_c at a radius of overdensity 200 is computed as

$$v_c \equiv \left(\frac{GM_{\text{halo}}}{R_{200}} \right)^{1/2} = \left[GM_{\text{halo}}^{2/3} \left(\frac{4\pi}{3} \bar{\rho} 200 \right)^{1/3} \right]^{1/2} \quad (14)$$

$$= 123.5 \left(\frac{M_{\text{halo}}}{10^{11} h^{-1} M_{\odot}} \right)^{1/3} \left(\frac{1+z}{4} \right)^{1/2} \text{ km s}^{-1} \quad (15)$$

for our flat Λ cosmology and $\bar{\rho}$ is the mean density of the universe at redshift z .

Figure 4 shows the cumulative distribution for the absolute value of DLA rate-of-incidence $dN/dz(< \mathcal{R}_{AB})$ as a function of apparent magnitude of host galaxies. The new observational estimate $\log(dN/dz) = 0.60 \pm 0.10$ at $z = 3$ obtained by Prochaska et al. (2005) using the SDSS Data Release 3 with a conservative $1-\sigma$ error bar is indicated by the yellow shaded region and a red central line. We find that the P3, Q3 and Q5 runs underpredict dN/dz . We will discuss this discrepancy further in Section 8.

It is clear from this figure that only a very small fraction of DLA incidence is associated with galaxies brighter than $\mathcal{R}_{AB} = 25.5$. This is more evident when we look at Figure 5 which shows the cumulative probability distribution of DLA incidence. In Figure 5a, we show a case where we normalize the cumulative distribution by the value at $M_{\text{halo}} = 10^{9.8} h^{-1} M_{\odot}$, or equivalently, where we assume that the halos less massive than the above value do not host DLAs at all. Here, we roughly reproduce the result of Haehnelt et al. (2000) where they adopted the cutoff circular velocity of 50 km s^{-1} which corresponds to $M_{\text{halo}} \simeq 10^{9.8} h^{-1} M_{\odot}$. Similarly to their result, we find that for this cutoff mass, only $10 - 20\%$ of DLA sight-lines are contributed by galaxies brighter than the spectroscopic limit $\mathcal{R}_{AB} = 25.5$, and $70 - 90\%$ of the DLA sight-lines are contributed by galaxies brighter than $\mathcal{R}_{AB} = 30$ magnitude.

However, according to the work of Nagamine et al. (2004a), halos with masses down to $10^{8.5} h^{-1} M_{\odot}$ (or equivalently $v_c = 18 \text{ km s}^{-1}$) contribute to the DLA cross section (see their Figure 2 & 3), so the cutoff velocity of 50 km s^{-1} adopted by Haehnelt et al. (2000) could be too high. In Figure 5b we show a case with cutoff halo mass $M_{\text{halo}} > 10^{8.5} h^{-1} M_{\odot}$. Here, less than 15% of DLAs are contributed by galaxies with $\mathcal{R}_{AB} < 25.5$, and $50 - 70\%$ by those with $\mathcal{R}_{AB} < 30$.

6. Impact parameter distribution

We also compute the impact parameter distribution (i.e., projected separation between DLA sight-lines and the nearest galaxy) using the full information in the SPH simulations. Nagamine et al. (2004a,b) calculated the neutral hydrogen column density N_{HI} for each pixel with a size of ϵ^2 on projected planes covering the face of each dark matter halo, where ϵ is the smoothing length of the simulation. Then, the pixels with $N_{\text{HI}} > 2 \times 10^{20} \text{ cm}^{-2}$ were equally regarded as DLA sight-lines. Therefore there are multiple DLA sight-lines per halo. Our simulation generates star particles according to the subparticle multiphase interstellar model of Springel & Hernquist (2003a), therefore galaxies are identified in the simulation as collections of star particles. Nagamine et al. (2004d,c) computed the spectrophotometric properties of simulated galaxies based on the formation time, stellar mass, and metallicity of individual star particles, and showed that the simulated luminosity functions agree well with the observations if a mean extinction of $E(B - V) = 0.15$ is assumed. This level of extinction is consistent with observationally derived values for the Lyman break galaxies (LBGs) at $z \sim 3$ (Shapley et al. 2001).

Knowing the locations of both DLAs and galaxies in the simulation, we compute the impact parameter for each DLA pixel by searching for the nearest galaxy on the projected plane. If a nearby galaxy cannot be found within the same halo, we allow the search to extend

further. Figure 6 shows the cumulative probability distribution of DLA rate-of-incidence as a function of impact parameter b_{phys} (in units of physical h_{70}^{-1} kpc). Figure 6a shows the results of the O3, P3, and Q3 runs to highlight the impact of galactic wind feedback. As the feedback strength increases, gas in low mass halos is ejected more efficiently, and the neutral hydrogen content decreases. Therefore, the relative contribution from higher mass halos increases and the impact parameter distribution becomes broader because the galaxies in massive halos are generally larger than those in lower mass halos. Another notable feature of this plot is that, if all galaxies are allowed to be a candidate DLA galaxy no matter how faint they are, then the majority (over 90% for the O3 run and 80% for the P3 and Q3 runs) of DLA sight-lines have the nearest galaxy within $b_{\text{phys}} = 5 h_{70}^{-1}$ kpc. However, if we limit the search for the nearest galaxy to those brighter than $\mathcal{R}_{AB} = 30$ or 28 mag, then a large fraction of DLAs, in particular those in low mass halos, cannot be associated with a qualified galaxy within the same halo, resulting in a much broader impact parameter distribution. About 30% of all DLA sight-lines in the O3 run have impact parameters $b_{\text{phys}} > 5 h_{70}^{-1}$ kpc for the limited search of a nearest galaxy with $\mathcal{R}_{AB} < 28$.

Figure 6b shows the result of the Q3 and Q5 runs. The higher resolution run (Q5) has a narrower impact parameter distribution than the lower resolution run (Q3), because it can resolve more low-mass galaxies which host DLAs with low impact parameters. Therefore the relative contribution from DLAs with low impact parameters becomes larger. Also, galaxies in massive halos will be better resolved in the Q5 run than in the Q3 run, and this will also result in smaller impact parameters for the DLAs in massive halos. Similarly to the O3 run in panel (a), we also show the case where we limit the search for the nearest galaxy to those brighter than $\mathcal{R}_{AB} = 30$ mag. In this case, results from the Q3 and Q5 runs agree well, and about 40% of all DLA sight-lines have impact parameters $b_{\text{phys}} > 5 h_{70}^{-1}$ kpc.

For most of the DLAs with low impact parameters, there is a galaxy within the same dark matter halo. However, for a few to 10% of the DLA sight-lines that are in the low mass halos in O3, P3, and Q3 runs, there are no galaxies within the same halo and the nearest galaxy is in another halo, as indicated by the offset of the curves at the bottom right corner of the plot in panel (a). In the Q5 run, there are almost no DLA sight-lines that do not have a galaxy within the same halo; i.e., $P(b)$ approaches zero at large b_{phys} values in panel (b).

Overall, our impact parameter distribution seems to be much narrower than that obtained by Haehnelt et al. (2000) if we do not limit our search to the bright galaxies. Figure 3 of Haehnelt et al. (2000) suggests that 60% of DLA sight-lines have $b < 1$ arc second, but our results indicate that more than 80% of DLAs have $b < 1$ arc second if we do not limit our search for the nearest galaxy to those with $\mathcal{R}_{AB} < 30$ mag. The differences between the two results might owe to the subhalos within the massive halos in the simulations

which Haehnelt et al. (2000) did not take into account. The calculation of Haehnelt et al. (2000) assigns a single effective DLA radius to each halo and assumes that the DLAs cover a circular area centered on each halo, whereas in our simulations, massive halos contain numerous galaxies within themselves and the geometry of the DLA cross section cannot be characterized by a circular area centered on each halo. For example, the most massive halo in the O3 run contains 143 galaxies, and in the Q5 run 1110 galaxies. Therefore the DLAs in the simulation would be able to find the nearest galaxy at distances much smaller than the effective DLA radius computed by Haehnelt et al. (2000). But when we limit our search for the nearest galaxy to those with $\mathcal{R}_{AB} < 30$ mag, then our results for the Q3 and Q5 run become similar to that obtained by Haehnelt et al. (2000). It is not clear how our results compare to Figure 11d by Mo et al. (1998) as these authors only looked at the differential distribution of impact parameter and not the cumulative probability distribution. But their differential distribution peaks at $2.5 h^{-1}$ kpc and a significant fraction (more than 50%) of the area under the curve appears to come from $b < 5 h^{-1}$ kpc, in better agreement with our results.

7. Number density of DLAs

Finally, we discuss the comoving number density of DLAs. Assuming that the characteristic covering area of each DLA A_{DLA} is fixed with a physical radius r_{DLA} (i.e., $A_{\text{DLA}} = \pi r_{\text{DLA}}^2$), we can compute the cumulative number density of DLAs as a function of halo mass using Equation (1):

$$N_{\text{DLA}}(> M) = \int_M^\infty dM n(M) \frac{\sigma_{\text{DLA}}^{\text{phys}}}{A_{\text{DLA}}}, \quad (16)$$

where the definitions of $n(M)$ and $\sigma_{\text{DLA}}^{\text{phys}}$ are the same as described in Section 3. Note again that σ_{DLA} is the *total* DLA cross section of each dark matter halo; in other words, if there are 100 DLAs in a massive halo, then this halo has a total DLA cross section of $\sigma_{\text{DLA}}^{\text{phys}} = 100 A_{\text{DLA}}$. Then, using Equation (11) allows us to obtain the cumulative comoving number density of DLAs as a function of apparent \mathcal{R}_{AB} magnitude $N_{\text{DLA}}(< \mathcal{R}_{AB})$ as shown in Figure 7. Here, three different values of physical radius for DLAs are assumed: $r_{\text{DLA}} = 1, 5$ and $20 h_{70}^{-1}$ kpc. For each radius, the results of four simulations (O3, P3, Q3, and Q5 runs) are shown. Also given is the cumulative number density of LBGs $N_{\text{LBG}}(< m)$ computed by integrating the Schechter luminosity function of Adelberger & Steidel (2000) with parameters $(m^*, \alpha, \Phi^*[h^3 \text{Mpc}^{-3}]) = (24.54, -1.57, 4.4 \times 10^{-3})$:

$$N_{\text{LBG}}(< m) = \int_m^0 \Phi(m) dm, \quad (17)$$

where $\Phi(m) = (0.4 \ln 10) \Phi^* 10^{\mu(\alpha+1)} \exp(-10^\mu)$ as a function of apparent magnitude m , and $\mu = 0.4(m^* - m)$. The comoving number density of LBGs at $z = 3$, $N_{\text{LBG}} = 4 \times 10^{-3}$ (Adelberger et al. 2003), is also shown as the data point at the magnitude limit of $\mathcal{R}_{AB} = 25.5$.

Figure 7 shows that the comoving number density of DLAs is larger than that of LBGs down to the magnitude limit of $\mathcal{R}_{AB} = 25.5$ if the physical radius of each DLA is smaller than $r_{\text{DLA}} \simeq 5 h_{70}^{-1} \text{kpc}$. The two number densities roughly agree with each other at $\mathcal{R}_{AB} = 25.5$ when $r_{\text{DLA}} \simeq 20 h_{70}^{-1} \text{kpc}$. Earlier, Schaye (2001) argued that the observed DLA rate-of-incidence can be accounted for if each LBG were accompanied by a DLA cross section of $\pi r^2 = \pi(19h^{-1} \text{kpc})^2$ assuming $(dN/dz)_{\text{DLA}} = 0.20$ and $N_{\text{LBG}} = 0.016 h^3 \text{Mpc}^{-3}$ (down to $\mathcal{R}_{AB} = 27$ mag). His result is in good agreement with the result of Q5 run with $r_{\text{DLA}} = 20 h_{70}^{-1} \text{kpc}$ shown in Figure 7. However, this large DLA radius is somewhat unrealistic because this model implies that all halos with masses $M_{\text{halo}} \gtrsim 10^{12} h^{-1} M_\odot$ host such a large disk at $z = 3$ that are responsible for DLAs, and none of the less massive halos host DLAs at all. This picture is quite the contrary to our simulation results that indicate halos down to masses $M_{\text{halo}} = 10^{8.5} h^{-1} M_\odot$ could host DLAs, and simulated DLAs in lower mass halos are clumpy and smaller in size.

The existence of extended disks at high redshift can be observationally tested by searching for extended emission from stars in deep imaging data such as the Hubble Deep Fields (Bouwens et al. 2003; Ferguson et al. 2004). The most recent study on this issue by Bouwens et al. (2004) using the Hubble Ultra Deep Field (HUDF) suggests that high-redshift $UBVi$ -dropout galaxies are compact in size ($\sim 0.1 - 0.3$ arc seconds) and that large ($\gtrsim 0.4$ arc sec, $\gtrsim 3$ kpc) are rare. Another observational analysis of high-redshift galaxies in HUDF by Chen & Wolfe (2005, in preparation) also suggests that there are no extended disks down to very faint surface brightness. Our simulation results and impact parameter distribution are in accord with these observational results. If our picture is realistic and each DLA has a physical size of $\lesssim 5$ kpc, then it means that there are multiple clumps of DLAs around massive galaxies such as LBGs at $z \sim 3$, although the fraction of DLA incidence covered by the DLAs in massive halos ($M_{\text{halo}} \gtrsim 10^{12} h^{-1} M_\odot$) is smaller than that in less massive halos that host very faint galaxies ($\mathcal{R}_{AB} \gtrsim 27$ mag).

8. Discussion & Conclusions

Using state-of-the-art cosmological SPH simulations, we have examined the distribution of DLA rate-of-incidence as a function of halo mass, galaxy apparent magnitude, and impact parameter. We find that the majority of DLA rate-of-incidence in the simulations

is dominated by relatively lower mass halos ($M_{\text{halo}} < 10^{12} h^{-1} M_{\odot}$) and faint ($\mathcal{R}_{AB} > 25.5$) galaxies. This conclusion agrees with the generic prediction of the semi-analytic model of Kauffmann (1996), that the DLA galaxies at high redshift will typically be smaller, more compact, and less luminous than disk galaxies at the present epoch, although this analysis was restricted to an $\Omega_m = 1$ universe. More recent work by Okoshi & Nagashima (2005) also suggests that the low-redshift ($z \leq 1$) DLA galaxies are mainly low-luminosity, compact galaxies. Combined with our results, the dominance of faint galaxies in DLA incidence seems to be a generic prediction of a CDM model. This can be ascribed to the steeply rising dark matter halo mass function towards lower masses in CDM models, and to the fact that the small DLA cross sections in these low mass halos add up to a large portion of the total DLA incidence when multiplied by a large number of low-mass halos.

8.1. On the DLA Halo Mass

We characterize the differential distribution of DLA rate-of-incidence $dN/(dz d \log M)$ with various halo masses listed in Table 2. We find that the mean DLA halo mass increases with increasing galactic wind feedback strength, because winds are able to eject the gas in lower mass halos, suppressing their DLA cross section, resulting in a larger relative contribution from higher mass halos (see also Nagamine et al. 2004a). The mean DLA halo mass for the Q5 run was found to be $\langle M_{\text{DLA}} \rangle = 10^{12.4} h^{-1} M_{\odot}$ and $\langle \log M_{\text{DLA}} \rangle = 10^{11.3} h^{-1} M_{\odot}$ when we limit the DLA distribution to $M_{\text{halo}} > 10^{8.5} h^{-1} M_{\odot}$. The latter value is close to that obtained by Bouche et al. (2005, $\langle \log M_{\text{DLA}} \rangle = 11.13$), but this comparison is not fully appropriate because their simulation could only resolve halos with masses $\log M_{\text{halo}} > 10.7$ and they did not attempt to extrapolate their halo distribution using an analytic halo mass function. Therefore, their mean DLA halo mass is biased towards a larger value ($\log M_{\text{DLA}} \gtrsim 11$) owing to limited resolution. Since their simulation did not include galactic wind feedback and also in terms of resolution, it is similar to that of our O3 ('no-wind') run. In fact, the value of concern for the O3 run is $\langle \log M_{\text{DLA}} \rangle = 10.4$ when we take the full distribution of DLAs into account down to $M_{\text{halo}} = 10^{8.5} h^{-1} M_{\odot}$, and it is lower than their halo mass resolution. We also note that there are large differences between $\langle \log M_{\text{DLA}} \rangle$, $\log \langle M_{\text{DLA}} \rangle$, & M_{50} , and therefore the former two quantities are not to be confused with M_{50} .

There have already been several observational attempts to constrain DLA halo masses via cross-correlation between DLAs and LBGs (Gawiser et al. 2001; Adelberger et al. 2003; Bouche & Lowenthal 2003, 2004), but owing to limited sample sizes, the results have been mostly inconclusive. More recently, Cooke (2005) has measured the cross-correlation between 11 DLAs and 211 LBGs, and constrained the DLA halo mass to be $\approx 10^{11.2} M_{\odot}$. It is

encouraging that this measurement is close to our results listed in Table 2. We should not over-interpret the observational results yet as they are still preliminary, but it suggests that at least some DLAs are associated with relatively massive halos, close to LBG halo masses ($\sim 10^{12} M_{\odot}$). There could of course be some distribution in the LBG halo masses (perhaps from $M_{\text{halo}} = 10^{10}$ to $10^{13} M_{\odot}$; see the broad distribution of stellar masses at the magnitude limit $\mathcal{R}_{AB} = 25.5$ in Figure 4 of Nagamine et al. (2004d)), and likewise DLAs could also have a broad halo mass distribution as we discussed in this paper. We note, again, that the majority of DLA sight-lines in the simulations are dominated by lower mass halos in spite of a relatively large mean DLA halo mass, which is also reflected in the large differences between the median halo mass and the mean halo mass as we summarize in Table 2.

8.2. On the Luminosity Distribution

As for the luminosity distribution of DLA galaxies, we find that only about 10% of DLA sight-lines are associated with galaxies brighter than $\mathcal{R}_{AB} = 25.5$ mag. This suggests that only about 10% of DLA galaxies will be found in searches for the bright LBGs at $z \sim 3$ down to $\mathcal{R}_{AB} = 25.5$. We reproduce the result of Haehnelt et al. (2000) when we cut our DLA distribution at $M_{\text{halo}} = 10^{9.8} h^{-1} M_{\odot}$ (or equivalently a circular velocity of $v_c = 50 \text{ km s}^{-1}$), and in this case 70 – 90% of DLA sight-lines are associated with galaxies brighter than $\mathcal{R}_{AB} = 30$ mag. This agreement with the Haehnelt et al. result is not surprising, because they assumed a relation $\sigma_{\text{DLA}} \propto v_c^{\alpha} \propto M_{\text{halo}}^{\alpha/3}$ with $\alpha \sim 2.5 – 3$ and a normalization matched to the observed dN/dz of DLAs, and our SPH simulations suggest $\alpha = 2.2 – 3.1$, depending on the feedback strength and resolution, and are able to reproduce the observed dN/dz (Nagamine et al. 2004a). However, our simulations indicate that even lower mass halos contribute to the DLA cross section, and when we cut our DLA distribution at $M_{\text{halo}} = 10^{8.5} h^{-1} M_{\odot}$, only 50 – 70% of DLAs are associated with galaxies brighter than $\mathcal{R}_{AB} = 30$ mag. Thus, it would be possible to detect DLA galaxies with $\sim 50\%$ efficiency by going down to $\mathcal{R}_{AB} = 30$ mag.

While the dominance of faint galaxies among DLAs seems to be a generic prediction of the CDM model, we note that the recent photometric survey of low-redshift ($z < 1$) DLA galaxies by Chen & Lanzetta (2003) on the contrary suggests that a large contribution from dwarf galaxies is not necessary to account for their observed DLA rate-of-incidence. However, this conclusion might be affected by the ‘masking effect’ emphasized by Okoshi & Nagashima (2005), where current DLA surveys could be biased against the detection of DLAs associated with faint and compact galaxies because such galaxies would be buried under the bright QSO that has to be masked for the detection of a DLA galaxy. This effect

would be more severe if the impact parameters are small as our present work suggests, as well as some observational studies of high-redshift DLA galaxies that imply very small impact parameters less than several kpc (i.e., $\lesssim 1$ arcsec) (Fynbo et al. 1999; Kulkarni et al. 2000; Møller et al. 2002, 2004). Fynbo et al. (1999) suggests that, based on the properties of a limited sample of observed high redshift candidate DLA galaxies, a large fraction ($\sim 70\%$) of DLA galaxies at $z \simeq 3$ could be fainter than $\mathcal{R}_{AB} = 28$ mag. It is possible that evolution with redshift is fairly strong as suggested by the chemical evolution model of Lanfranchi & Friaca (2003), in the sense that the high-redshift DLAs are dominated by dwarf galaxies and the low-redshift ones by disks. But the latter scenario seems to be inconsistent with the predictions of Okoshi & Nagashima (2005).

Hopkins et al. (2005) also argued for the dominance of faint galaxies for the DLA galaxies based on the comparison of global quantities such as the density of gas mass, stellar mass, metal mass, and star formation rate. They also suggested that the DLAs may be a distinct population from LBGs, but we note that the dominance of faint galaxies for the DLA rate-of-incidence does not immediately mean that DLAs do not exist in LBGs. It simply means that the area covered by the DLAs associated with LBGs is much smaller than that in faint galaxies. We plan to investigate the connection between DLAs and LBGs in more detail in future work.

8.3. On the Impact Parameter Distribution

Our distribution of impact parameters is significantly narrower than that of Haehnelt et al. (2000), and we ascribe this difference to substructures within the massive halos in our simulations. The differential distribution of Mo et al. (1998, Figure 11d) seems to be in better agreement with our results, with roughly half of DLAs having $b_{\text{phys}} < 3h^{-1}$ kpc, but this comparison is probably not fully appropriate because their model is restricted to centrifugally supported disks. Indeed, Haehnelt et al. (2000) comment in their paper that their effective DLA radius is about a factor of 10 larger than the expected scale length of a centrifugally supported disk if the angular momentum of the gas owes to tidal torquing during the collapse of a dark matter halo. However, we caution that the large effective DLA radius for a massive halo does not necessarily mean that DLAs consist of only large disks centered on halos; i.e., the DLA cross section could be distributed to hundreds of galaxies (associated with subhalos) embedded in a massive halo, with each DLA being fairly compact. This point was also emphasized by Gardner et al. (2001, Section 4.1).

Our narrow impact parameter distribution at first sight might seem inconsistent with that of Gardner et al. (2001), but in fact they are not. Gardner et al. (2001) mostly

used SPH simulations with 64^3 particles which were able to resolve halos only down to $M_{\text{halo}} = 8.2 \times 10^{10} M_{\odot}$, and found that nearly all DLAs lie within $15 - 20$ kpc of a galaxy center. Given their mass resolution, they were not able to simulate galaxies fainter than $\mathcal{R}_{AB} \simeq 30$ mag at $z = 3$. If we limit the search for the nearest galaxy to those brighter than $\mathcal{R}_{AB} = 30$ mag (see Figure 6b), our simulations suggest that 80% of DLAs are within $b_{\text{phys}} = 15 h_{70}^{-1}$ kpc, which is not so different from the results of Gardner et al. (2001). However if we include the fainter galaxies that were not resolved in the simulations by Gardner et al. (2001), then the overall impact parameter distribution quickly becomes narrow, with more than 80% of DLA sight-lines having $b_{\text{phys}} < 5 h_{70}^{-1}$ kpc. In addition to the significant improvement in resolution, our simulations also employ a novel entropy-conserving formulation of SPH (Springel & Hernquist 2002) which takes variations of the SPH smoothing lengths into account self-consistently. These multiple improvements of the SPH simulations over the past few years, including the treatment of galactic wind feedback, are probably the primary cause for differences with earlier numerical works.

The small impact parameters suggest that DLAs in our simulations are compact, and this has significant implications for the nature of DLAs. The compactness of the simulated DLAs can also be observed in the projected distribution of DLAs in Figure 2 & 3 of Nagamine et al. (2004b). There, one can see that the DLAs are at the centers of galaxies and coincide with star-forming regions quite well, covering roughly half the area of the star-forming region. These results are at odds with the idea that DLAs mainly originate from gas in large galactic disks (e.g., Wolfe et al. 1986; Turnshek et al. 1989; Prochaska & Wolfe 1997, 1998). The overall agreement between the simulations and observations found by Nagamine et al. (2004a,b) was encouraging, but the simulations with galactic wind feedback now seem to underpredict the DLA rate-of-incidence (see Figure 4) compared to the new observational estimate by Prochaska et al. (2005) utilizing the SDSS Data Release 3. As both Wolfe et al. (2005) and Prochaska et al. (2005) point out, this is because our simulations underpredict the column density distribution $f(N_{\text{HI}})$ at $20 < \log N_{\text{HI}} < 21$ by a factor of $2 - 3$ even in our highest resolution run with a smoothing length of comoving $1.23 h^{-1}$ kpc. Cen et al. (2003) reported that they did not have this problem, but instead they significantly overpredicted $f(N_{\text{HI}})$ at $\log N_{\text{HI}} > 22$ as well as Ω_{gas} , and had to introduce dust extinction to match observations. Furthermore, this inconsistency in the column density distribution between SPH simulations and observations and the compactness of the simulated DLAs might be related to the well-known angular momentum problem (Robertson et al. 2004, and references therein) in hydrodynamic simulations of disk galaxy formation, where simulated disk galaxies are known to be too small and centrally concentrated. This is a problem that is not easy to solve, and future studies are needed using both Eulerian mesh simulations and SPH simulations. In summary, there persists a tension between the predicted and observed

$f(N_{\text{HI}})$, large observed velocity widths (which favors large and thick disks), and the predicted compactness of DLAs (cf. Jedamzik & Prochaska 1998).

Acknowledgements

We thank Jeff Cooke and Jason Prochaska for useful discussions. This work was supported in part by NSF grants ACI 96-19019, AST 00-71019, AST 02-06299, and AST 03-07690, and NASA ATP grants NAG5-12140, NAG5-13292, and NAG5-13381. The simulations were performed at the Center for Parallel Astrophysical Computing at the Harvard-Smithsonian Center for Astrophysics.

REFERENCES

Adelberger, K. L. & Steidel, C. C. 2000, ApJ, 544, 218

Adelberger, K. L., Steidel, C. C., Shapley, A. E., & Pettini, M. 2003, ApJ, 584, 45

Bouche, N., Gardner, J. P., Weinberg, D. H., Davé, R., & Lowenthal, J. D. 2005, ApJ, 628, 89

Bouche, N. & Lowenthal, J. D. 2003, ApJ, 596, 810

—. 2004, ApJ, 609, 513

Bouwens, R. J., Blakeslee, J. P., Illingworth, G. D., Broadhurst, T. J., & Franx, M. 2004, ApJ, 611, L1

Bouwens, R. J., Broadhurst, T. J., & Illingworth, G. D. 2003, ApJ, 593, 640

Bruzual, G. & Charlot, S. 2003, MNRAS, 344, 1000

Cen, R., Nagamine, K., & Ostriker, J. P. 2004, ApJ, in press (astro-ph/0407143)

Cen, R., Ostriker, J. P., Prochaska, J. X., & Wolfe, A. M. 2003, ApJ, 598, 741

Chen, H.-W. & Lanzetta, K. M. 2003, ApJ, 597, 706

Cooke, J. 2005, PhD thesis, University of California, San Diego

Davé, R., Hernquist, L., Katz, N., & Weinberg, D. H. 1999, ApJ, 511, 521

Davis, M., Efstathiou, G., Frenk, C. S., & White, S. D. M. 1985, *ApJ*, 292, 371

Efstathiou, G., Bond, J. R., & White, S. D. M. 1992, *MNRAS*, 258, 1

Eisenstein, D. & Hu, P. 1999, *ApJ*, 511, 5

Ferguson, H. C., Dickinson, M., Giavalisco, M., Kretchmer, C., Ravindranath, S., Idzi, R., Taylor, E., Conselice, C. J., et al. 2004, *ApJ*, 600, L107

Fynbo, J. U., Møller, P., & Warren, S. J. 1999, *MNRAS*, 305, 849

Gardner, J., Katz, N., Hernquist, L., & Weinberg, D. H. 1997a, *ApJ*, 484, 31

—. 2001, *ApJ*, 559, 131

Gardner, J., Katz, N., Weinberg, D. H., & Hernquist, L. 1997b, *ApJ*, 486, 42

Gawiser, E., Wolfe, A. M., Prochaska, J. X., Lanzetta, K. M., Yahata, N., & Quirrenbach, A. 2001, *ApJ*, 562, 628

Haardt, F. & Madau, P. 1996, *ApJ*, 461, 20

Haehnelt, M., Steinmetz, M., & Rauch, M. 1998, *ApJ*, 495, 647

—. 2000, *ApJ*, 534, 594

Hopkins, A. M., Rao, S. M., & Turnshek, D. A. 2005, *ApJ*, 630, 108

Jedamzik, K. & Prochaska, J. X. 1998, *MNRAS*, 296, 430

Katz, N., Weinberg, D. H., & Hernquist, L. 1996a, *ApJS*, 105, 19

Katz, N., Weinberg, D. H., Hernquist, L., & Miralda-Escudé, J. 1996b, *ApJ*, 457, L57

Kauffmann, G. 1996, *MNRAS*, 281, 475

Kulkarni, V. P., Hill, J. M., Schneider, G., Weymann, R. J., Storrie-Lombardi, L. J., Rieke, M., Thompson, R. I., & Jannuzi, B. T. 2000, *ApJ*, 536, 36

—. 2001, *ApJ*, 551, 37

Lanfranchi, G. A. & Friaca, A. C. S. 2003, *MNRAS*, 343, 481

Lanzetta, K. M., Wolfe, A. M., & Turnshek, D. A. 1995, *ApJ*, 440, 435

Le Brun, V., Bergeron, J., Boissé, P., & Deharveng, J. M. 1997, *A&A*, 321, 733

Maller, A., Prochaska, J. X., Somerville, R. S., & Primack, J. 2001, *ApJ*, 326, 1475

Mo, H. J., Mao, S., & White, S. D. M. 1998, *MNRAS*, 295, 319

Møller, P., Fynbo, J. U., & Fall, S. M. 2004, *A&A*, 422, L33

Møller, P., Warren, S. J., Fall, S. M., Fynbo, J. U., & Jakobsen, P. 2002, *ApJ*, 574, 51

Nagamine, K., Springel, V., & Hernquist, L. 2004a, *MNRAS*, 348, 421

—. 2004b, *MNRAS*, 348, 435

Nagamine, K., Springel, V., Hernquist, L., & Machacek, M. 2004c, *MNRAS*, 355, 638

—. 2004d, *MNRAS*, 350, 385

Nagashima, M., Totani, T., Gouda, N., & Yoshii, Y. 2001, *ApJ*, 557, 505

Night, C., Nagamine, K., Springel, V., & Hernquist, L. 2005, *MNRAS*, in press (astro-ph/0503631)

Okoshi, K. & Nagashima, M. 2005, *ApJ*, 623, 99

Okoshi, K., Nagashima, M., Gouda, N., & Yoshioka, S. 2004, *ApJ*, 603, 12

Péroux, C., McMahon, R. G., Storrie-Lombardi, L. J., & Irwin, M. J. 2003, *MNRAS*, 346, 1103

Prochaska, J. X., Herbert-Fort, S., & Wolfe, A. M. 2005, *ApJ*, submitted

Prochaska, J. X. & Wolfe, A. M. 1997, *ApJ*, 487, 73

—. 1998, *ApJ*, 507, 113

—. 2002, *ApJ*, 566, 68

Prochaska, J. X., Wolfe, A. M., Tytler, D., Burles, S., et al. 2001, *ApJS*, 137, 21

Rao, S. M. & Turnshek, D. A. 2000, *ApJS*, 130, 1

Robertson, B. E., Yoshida, N., Springel, V., & Hernquist, L. 2004, *ApJ*, 606, 32

Schaye, J. 2001, *ApJ*, 559, L1

Shapley, A. E., Steidel, C. C., Adelberger, K. L., Dickinson, M., Giavalisco, M., & Pettini, M. 2001, *ApJ*, 562, 95

Sheth, R. K. & Tormen, G. 1999, MNRAS, 308, 119

Somerville, R. S., Primack, J. R., & Faber, S. M. 2001, MNRAS, 320, 504

Springel, V. 2005, MNRAS, submitted (astro-ph/0505010)

Springel, V. & Hernquist, L. 2002, MNRAS, 333, 649

—. 2003a, MNRAS, 339, 289

—. 2003b, MNRAS, 339, 312

Springel, V., Yoshida, N., & White, S. D. M. 2001, New Astronomy, 6, 79

Storrie-Lombardi, L. J. & Wolfe, A. M. 2000, ApJ, 543, 552

Turnshek, D. A., Wolfe, A. M., Lanzetta, K. M., Briggs, F. H., Cohen, R. D., Foltz, C. B., Smith, H. E., & Wilkes, B. J. 1989, ApJ, 344, 567

Weatherley, S. J., Warren, S. J., Möller, P., Fall, S. M., Fynbo, J. U., & Croom, S. M. 2005, MNRAS, 358, 985

Wolfe, A. M., Gawiser, E., & Prochaska, J. X. 2005, ARA&A, 43, 861

Wolfe, A. M., Lanzetta, K. M., & Foltz, C. B. 1995, ApJ, 454, 698

Wolfe, A. M., Turnshek, D. A., Smith, H. E., & Cohen, R. S. 1986, ApJS, 61, 249

Table 1. Simulations

Run	N_p	m_{DM}	m_{gas}	ϵ	wind
O3	144^3	2.42×10^7	3.72×10^6	2.78	none
P3	144^3	2.42×10^7	3.72×10^6	2.78	weak
Q3	144^3	2.42×10^7	3.72×10^6	2.78	strong
Q4	216^3	7.16×10^6	1.10×10^6	1.85	strong
Q5	324^3	2.12×10^6	3.26×10^5	1.23	strong

Note. — Simulations employed in this study. All simulations have a comoving box-size of $10 h^{-1} \text{Mpc}$. The (initial) number of gas particles N_p is equal to the number of dark matter particles, so the total particle count is twice N_p . m_{DM} and m_{gas} are the masses of dark matter and gas particles in units of $h^{-1} M_\odot$, respectively, and ϵ is the comoving gravitational softening length in units of $h^{-1} \text{kpc}$. The value of ϵ is a measure of spatial resolution.

Table 2. DLA halo masses

Run	$\log M_{\text{peak}}$	$\log M_{50}$	$\log M_{75}$	$\log \langle M_{\text{DLA}} \rangle$	$\langle \log M_{\text{DLA}} \rangle$
O3	(8.5)	10.1	11.1	11.8	10.4
P3	9.6	10.4	11.5	11.9	10.6
Q3	10.8	10.7	11.7	12.0	10.8
Q4	11.6	11.1	12.0	12.2	11.1
Q5	12.0	11.5	12.3	12.4	11.3

Note. — Various DLA halo masses that characterize the differential distribution $dN/(dz d\log M)$ with the distribution cut-off at $M_{\text{halo}} = 10^{8.5} h^{-1} M_{\odot}$. The following quantities are listed: peak halo mass M_{peak} , median halo mass M_{50} (i.e., 50 percentile of the distribution), 75 percentile of the distribution M_{75} , mean halo mass $\langle M_{\text{DLA}} \rangle$ (Equation (8)), and the mean of $\log M_{\text{halo}}$ rather than M_{halo} itself for the comparison with the result by Bouche et al. (2005). The peak halo mass for O3 run is shown in the parenthesis because it is the cutoff mass itself of the distribution. All numbers are in units of $h^{-1} M_{\odot}$.

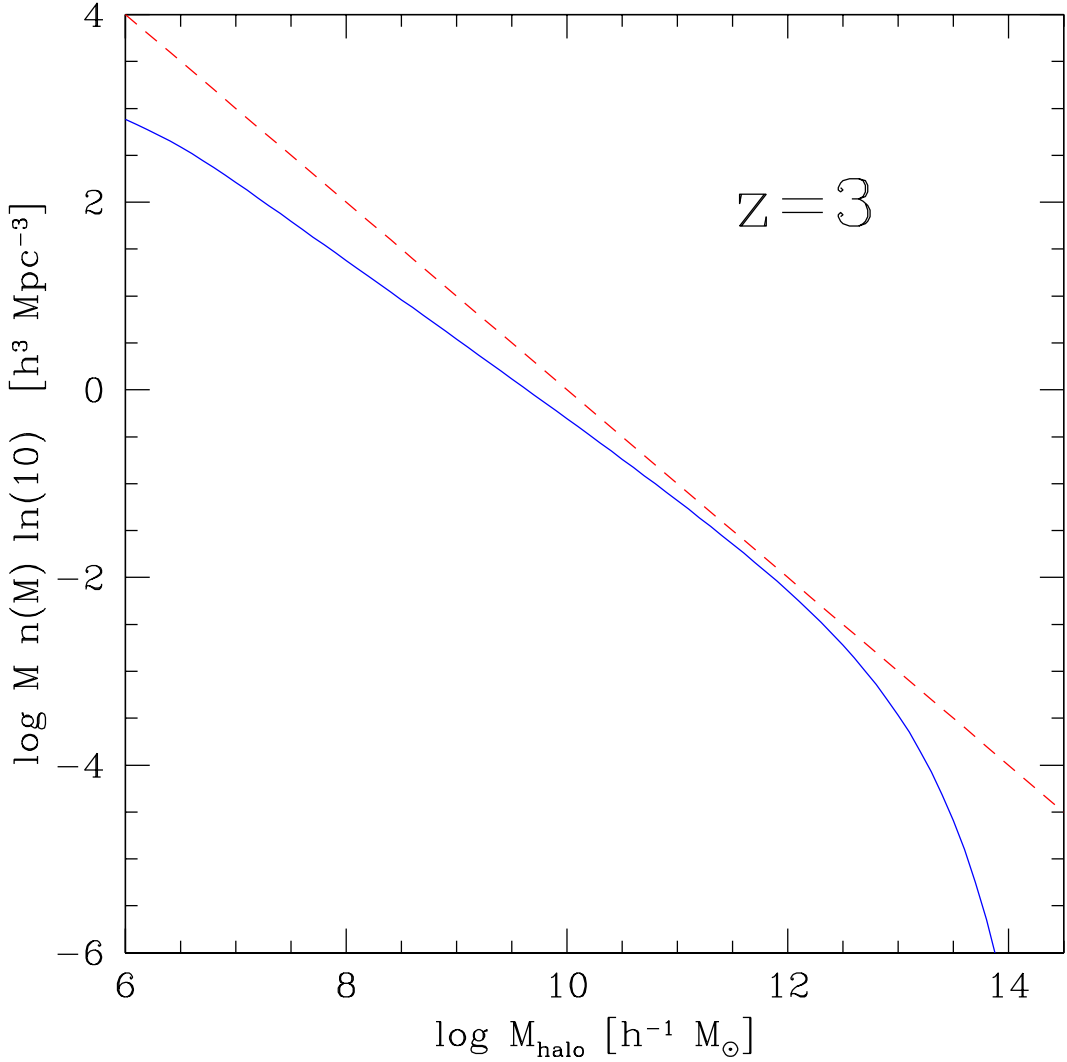


Fig. 1.— Dark matter halo mass function of Sheth & Tormen (1999) at $z = 3$, shown in the form of $M \cdot n(M)$ to ease the interpretation of Equation (2). The red dashed line shows a power-law $n(M) \propto M^{-2}$. We used the transfer function of Eisenstein & Hu (1999) and the power spectrum was normalized to $\sigma_8 = 0.9$ for the calculation. We have confirmed that the mass function does not change very much when the transfer function of Efstathiou et al. (1992) is used.

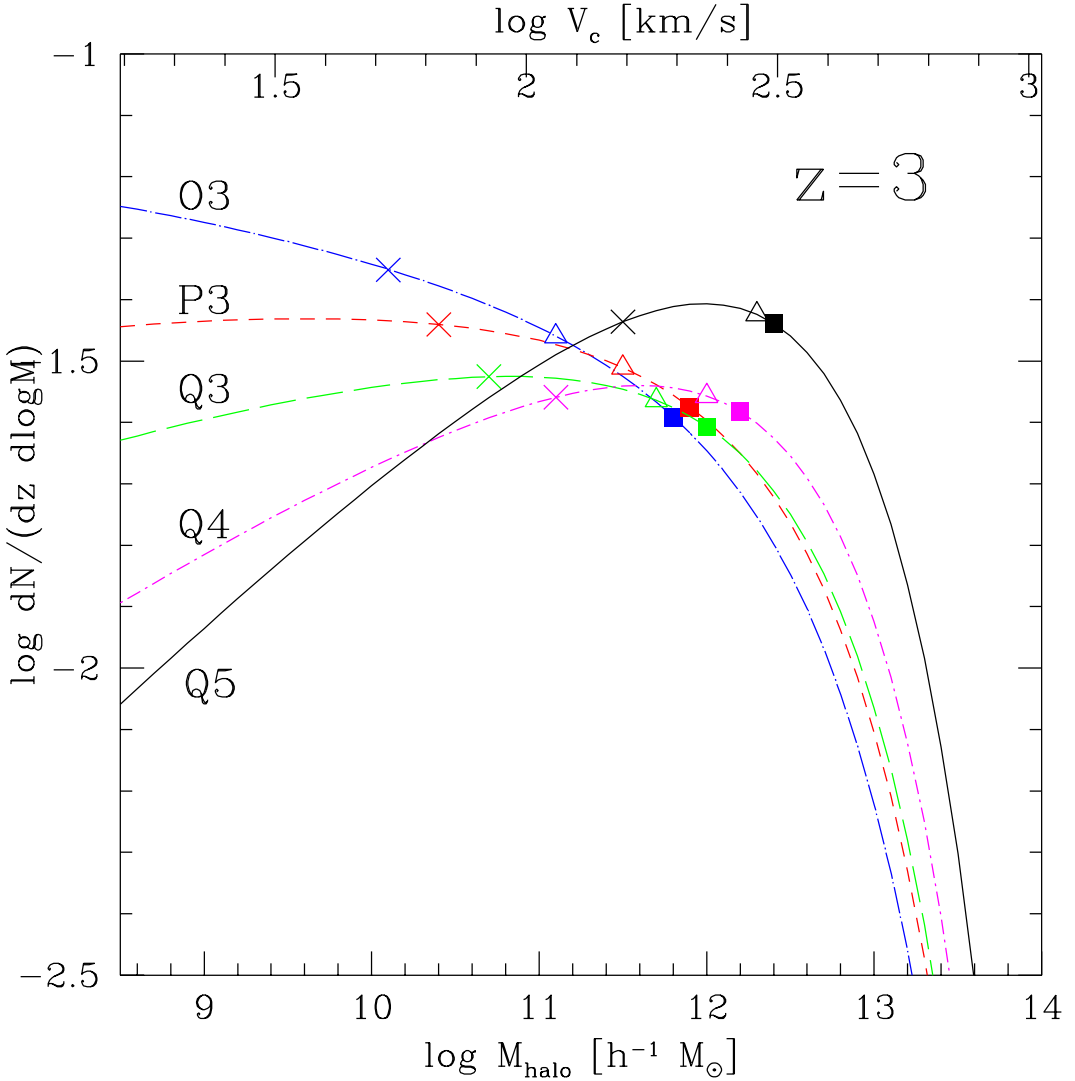


Fig. 2.— Differential distribution of DLA rate-of-incidence $dN/(dz d \log M)$ at $z = 3$ as a function of halo mass, computed using Equations (1) and (2). The open cross indicate the median halo masses M_{50} , and the open triangles indicate the 75 percentile of the distribution M_{75} . The filled squares indicate the mean DLA halo masses $\langle M_{\text{DLA}} \rangle$. The top axis also indicates the circular velocity as computed by Equation (15). The differences in the shape of the distribution arise from the differences in the relationships between DLA cross section and halo mass as summarized in Equation (1).

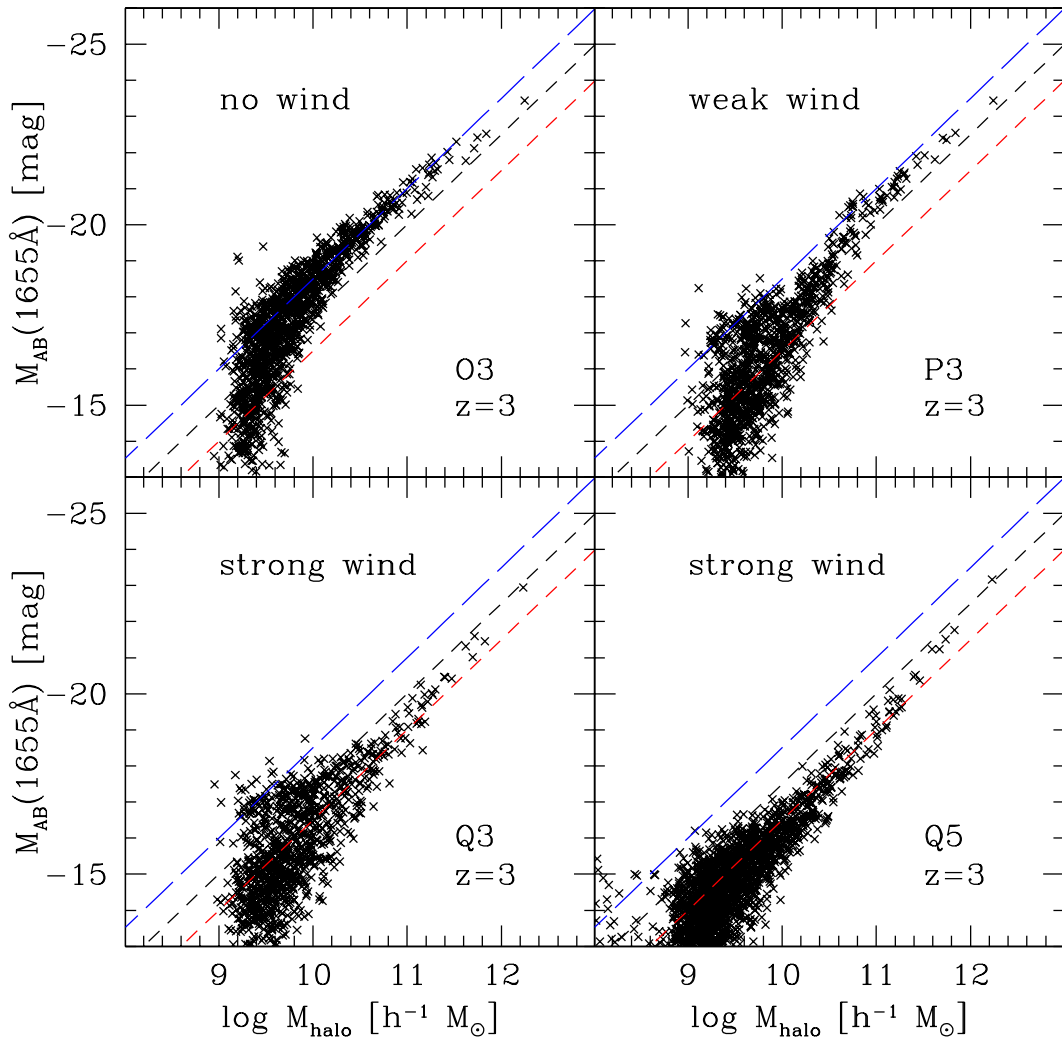


Fig. 3.— Halo mass vs. absolute AB magnitude at 1655Å at $z = 3$. See text for the description of the three dashed lines.

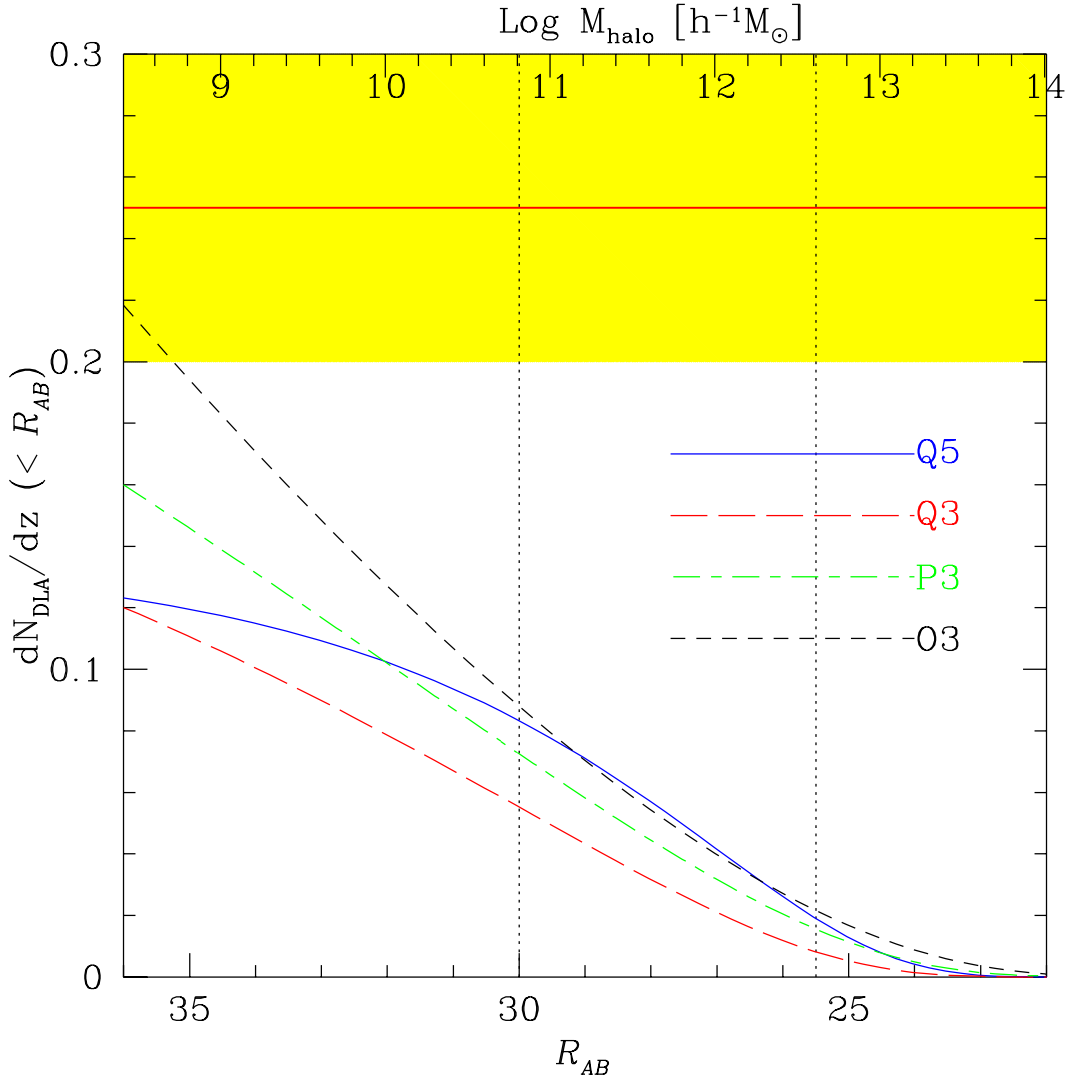


Fig. 4.— Cumulative distribution function of DLA rate-of-incidence as a function of apparent R_{AB} magnitude. The spectroscopic limit $R_{AB} = 25.5$ and the limiting magnitude of $R_{AB} = 30$ are indicated by the vertical dotted lines. The top axis gives the corresponding halo masses using the relationship for the Q3 and Q5 runs; $R_{AB} = -2.5 \log M_{\text{halo}} + 57.03 - 5 \log h_{70}$ (Equation (13)). The yellow band is the new observational estimate $\log(dN/dz) = 0.60 \pm 0.10$ at $z = 3$ by Prochaska et al. (2005) using the SDSS Data Release 3 with a conservative $1-\sigma$ error bar.

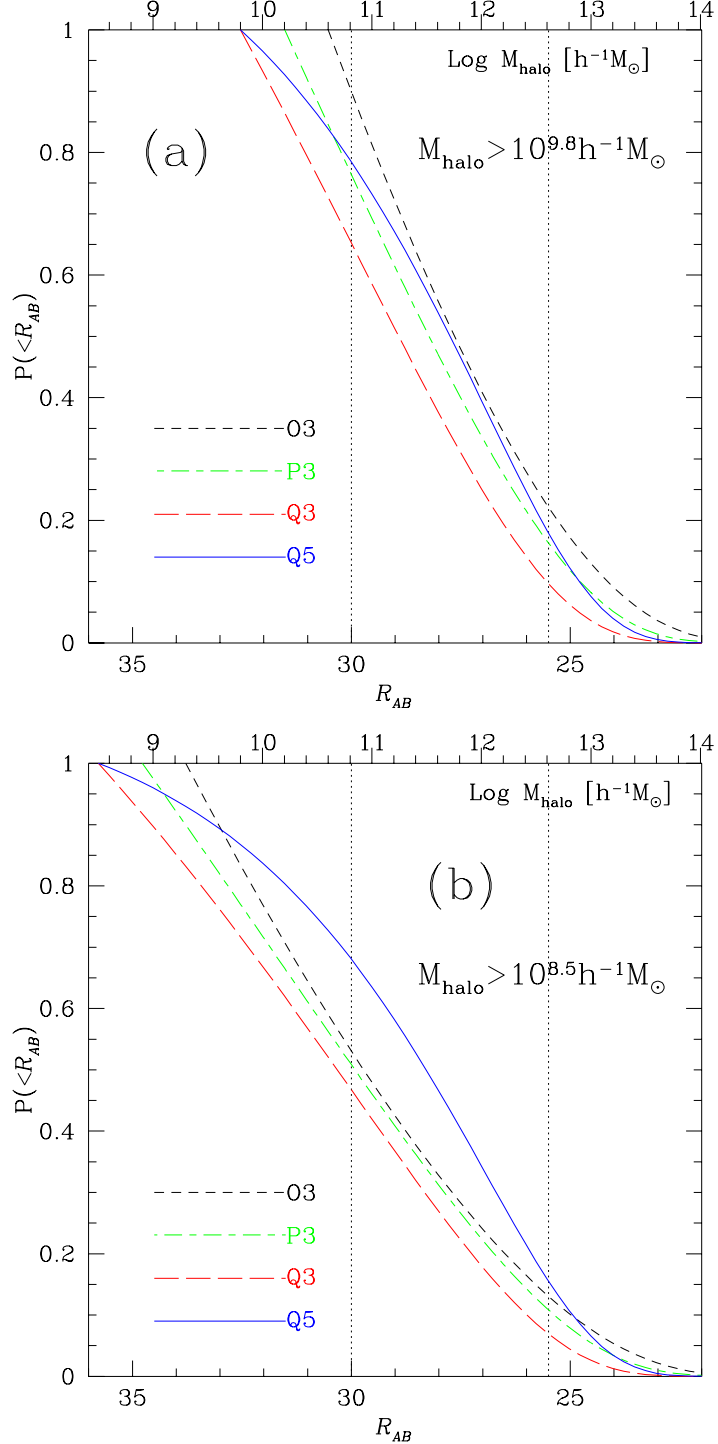


Fig. 5.— Cumulative probability distribution of DLA rate-of-incidence as a function of apparent \mathcal{R}_{AB} magnitude at $z = 3$. Panel (a) is when the distribution is normalized by the value at $M_{\text{halo}} = 10^{9.8} h^{-1} M_{\odot}$; i.e., assuming there would be no DLAs in halos less massive than this value. This roughly reproduces the result of Haehnelt et al. (2000). Panel (b) is when the distribution is normalized by the value at $M_{\text{halo}} = 10^{8.5} h^{-1} M_{\odot}$, which is more consistent with the results of our SPH simulations. The top axis shows the scaling with halo mass for the Q3 and Q5 runs, $\mathcal{R}_{AB} = -2.5 \log M_{\text{halo}} + 57.03 - 5 \log h_{70}$ (Equation 13).

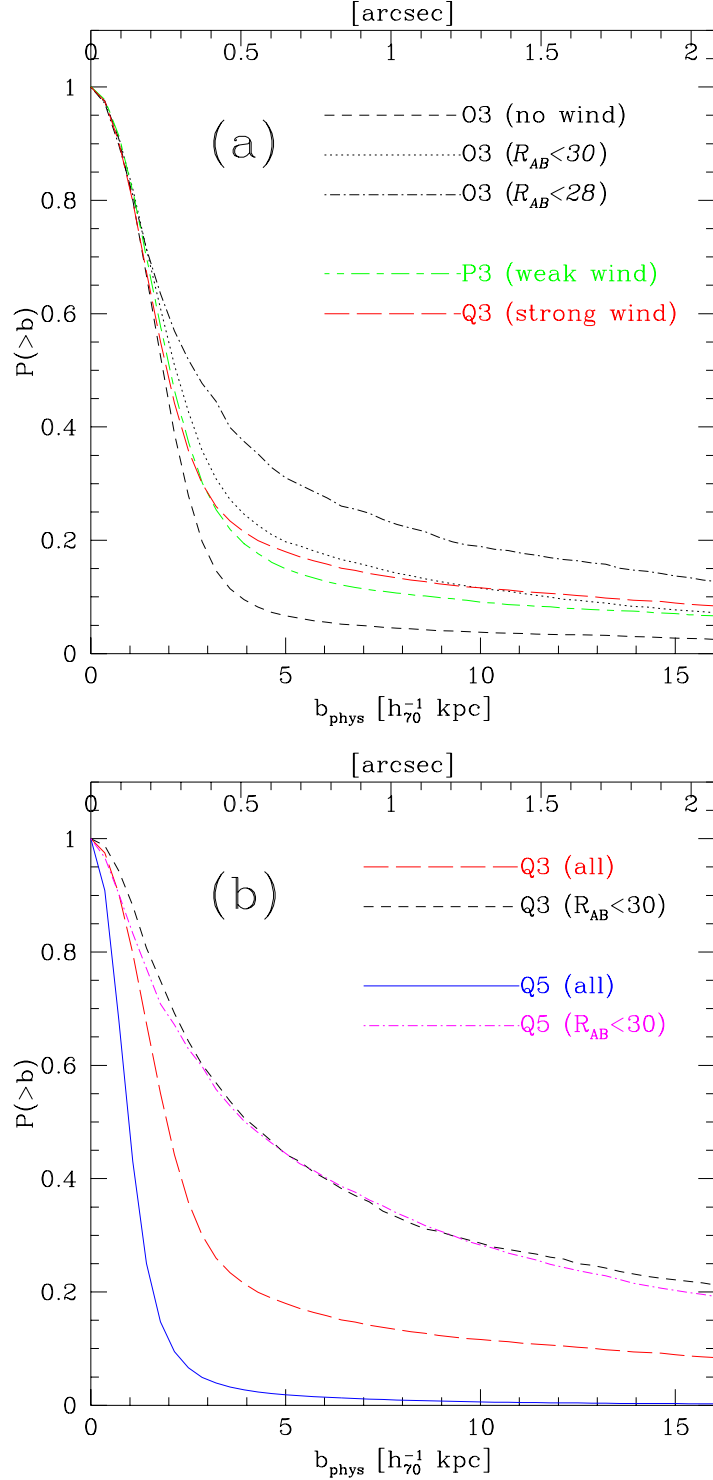


Fig. 6.— Cumulative probability distribution of DLA rate-of-incidence as a function of projected impact parameter d_{phys} in units of physical h_{70} kpc and angular scale in units of arc second at $z = 3$. *Panel (a)* shows the results of O3 (no wind), P3 (weak wind), and Q3 (strong wind) runs. *Panel (b)* shows the results of Q3 and Q5 runs. In both panels, we also show the results when the search for the nearest galaxy is limited to those brighter than a certain \mathcal{R}_{AB} magnitude.

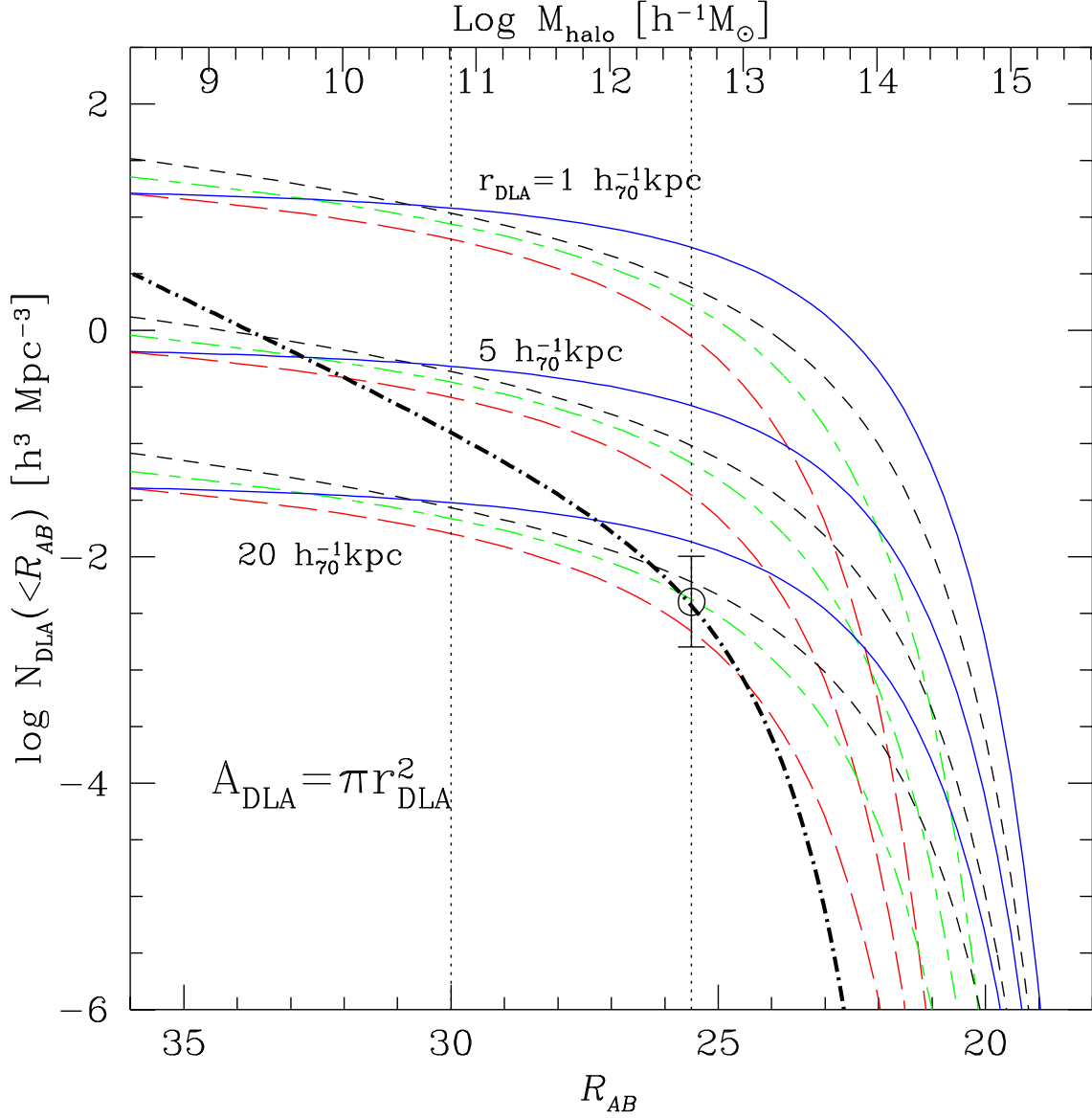


Fig. 7.— Cumulative, comoving number density of DLAs as a function of apparent \mathcal{R}_{AB} magnitude for 3 different values of assumed DLA physical radius $r_{\text{DLA}} = 1 h_{70}^{-1} \text{kpc}$, $5 h_{70}^{-1} \text{kpc}$, and $20 h_{70}^{-1} \text{kpc}$. The area of each DLA is $A_{\text{DLA}} = \pi r_{\text{DLA}}^2$. For each value of r_{DLA} , four different lines are shown: Q5 run (blue solid line), O3 (black dashed), P3 (green short-dash long-dash), and Q3 (red long-dashed). The thick black dot-dashed line is the cumulative comoving number density of LBGs obtained by integrating the observed luminosity function by Adelberger & Steidel (2000). The data point at $\mathcal{R}_{AB} = 25.5$ shows the comoving number density of LBGs $N_{\text{LBG}} = 4 \times 10^{-3} h^{-3} \text{Mpc}^{-3}$.